ANNALS of Clinical and Translational Neurology
Open Access
ANA American Neurological Association since 1875

RESEARCH ARTICLE

Vanishing white matter: deregulated integrated stress response as therapy target

Truus E. M. Abbink[1], Lisanne E. Wisse[1], Ermelinda Jaku[1], Michiel J. Thiecke[1,a], Daniel Voltolini-González[1], Hein Fritsen[1], Sander Bobeldijk[1], Timo J. ter Braak[1], Emiel Polder[1], Nienke L. Postma[1], Marianna Bugiani[1,2], Eduard A. Struijs[3], Mark Verheijen[4], Nina Straat[1,b], Sophie van der Sluis[5], Adri A. M. Thomas[6], Douwe Molenaar[7] & Marjo S. van der Knaap[1,8]

[1]Child Neurology, Emma Children's Hospital, Amsterdam University Medical Centers, Vrije Universiteit and Amsterdam Neuroscience, Amsterdam, The Netherlands
[2]Department of Pathology, Amsterdam University Medical Centers, Vrije Universiteit and Amsterdam Neuroscience, Amsterdam, The Netherlands
[3]Metabolic Unit, Department of Clinical Chemistry, Amsterdam University Medical Centers, Vrije Universiteit and Amsterdam Neuroscience, Amsterdam, The Netherlands
[4]Department of Molecular and Cellular Neurobiology, Center for Neurogenomics and Cognitive Research, Vrije Universiteit and Amsterdam Neuroscience, Amsterdam, The Netherlands
[5]Complex Trait Genetics, Department of Clinical Genetics, Center for Neurogenomics and Cognitive Research, Vrije Universiteit and Amsterdam Neuroscience, Amsterdam, The Netherlands
[6]Developmental Biology, Utrecht University, Utrecht, The Netherlands
[7]Systems Bioinformatics, Vrije Universiteit and Amsterdam Neuroscience, Amsterdam, The Netherlands
[8]Functional Genomics, Center for Neurogenomics and Cognitive Research, Vrije Universiteit and Amsterdam Neuroscience, Amsterdam, The Netherlands

Correspondence
Truus E. M. Abbink, De Boelelaan 1085 WN-A045, 1081 HV, Amsterdam, The Netherlands. Tel: +31 (0) 20 5988292; Fax: +31 (0)20 4440849; E-mail: g.abbink@amsterdamumc.nl

Present address
[a]Nuclear Dynamics Programme, The Babraham Institute, Babraham Research Campus, Cambridge, United Kindgdom
[b]Sylics, Amsterdam, The Netherlands

Funding information
None declared.

Received: 10 May 2019; Accepted: 31 May 2019

***Annals of Clinical and Translational Neurology* 2019; 6(8): 1407–1422**

doi: 10.1002/acn3.50826

Abstract

Objective: Vanishing white matter (VWM) is a fatal, stress-sensitive leukodystrophy that mainly affects children and is currently without treatment. VWM is caused by recessive mutations in eukaryotic initiation factor 2B (eIF2B) that is crucial for initiation of mRNA translation and its regulation during the integrated stress response (ISR). Mutations reduce eIF2B activity. VWM pathomechanisms remain unclear. In contrast with the housekeeping function of eIF2B, astrocytes are selectively affected in VWM. One study objective was to test our hypothesis that in the brain translation of specific mRNAs is altered by eIF2B mutations, impacting primarily astrocytes. The second objective was to investigate whether modulation of eIF2B activity could ameliorate this altered translation and improve the disease. **Methods**: Mice with biallelic missense mutations in eIF2B that recapitulate human VWM were used to screen for mRNAs with altered translation in brain using polysomal profiling. Findings were verified in brain tissue from VWM patients using qPCR and immunohistochemistry. The compound ISRIB (for "ISR inhibitor") was administered to VWM mice to increase eIF2B activity. Its effect on translation, neuropathology, and clinical signs was assessed. **Results**: In brains of VWM compared to wild-type mice we observed the most prominent changes in translation concerning ISR mRNAs; their expression levels correlated with disease severity. We substantiated these findings in VWM patients' brains. ISRIB normalized expression of mRNA markers, ameliorated brain white matter pathology and improved motor skills in VWM mice. **Interpretation**: The present findings show that ISR deregulation is central in VWM pathomechanisms and a viable target for therapy.

Introduction

Vanishing white matter (VWM) is a leukodystrophy, characterized by chronic neurological deterioration and episodes of rapid decline provoked by stresses, especially febrile infections.[1] Neuropathology shows white matter rarefaction and cystic degeneration with feeble astrogliosis, deficient myelin, and immature astrocytes and oligodendrocytes.[2] There is no cure for VWM and patients die prematurely.[1] Recessive mutations in any of the subunits of eukaryotic translation factor 2B (eIF2B), reducing its activity,[3,4] cause VWM.[5,6]

eIF2B is conditional for the initiation of translation of mRNAs into proteins, regulating protein synthesis rates and orchestrating the integrated stress response (ISR, Fig. 1A).[7] The ISR is activated by stressors, including oxidative stress, amino acid starvation, infections, and endoplasmic reticulum (ER) stress.[7] Homeostasis of the ER protein-folding environment is maintained by the unfolded protein response (UPR); the ISR is also one of the three UPR arms (Fig. 1A). ISR activation leads to phosphorylation of eIF2α, which sequesters eIF2B, thereby decreasing general mRNA translation rates and bulk protein synthesis, but increasing translation of specific mRNAs, such as *ATF4*, encoding transcription factor ATF4.[7]

VWM mouse models with homozygous (ho) mutations in eIF2Bδ (Arg484Trp) or eIF2Bε (Arg191His) subunits are representative of the human disease ($2b4^{ho}$ and $2b5^{ho}$ mice).[8] Crossbreeding generates $2b4^{he}2b5^{ho}$, $2b4^{ho}2b5^{he}$, and $2b4^{ho}2b5^{ho}$ (he, heterozygous) mice. Together they reproduce the clinical spectrum of human VWM with the following order of increasing severity: $2b4^{ho}$, $2b5^{ho}$, $2b4^{he}2b5^{ho}$/$2b4^{ho}2b5^{he}$, and $2b4^{ho}2b5^{ho}$, as reflected by earlier disease onset, severer motor dysfunction, lower body weight, shorter life span, and severer brain pathology.[8] Using these mice, we previously showed that astrocytes are the primarily affected cell type.[8] In our study, we reveal a constitutive enhanced expression of ATF4-regulated mRNAs indicative of deregulated ISR homeostasis, strikingly in astrocytes only, both in VWM mice and patients. ISRIB, an ISR inhibitor,[9] ameliorates both ISR deregulation in brain and the clinical disease in VWM mice.

Results

Increased expression of ATF4-driven transcriptome in $2b5^{ho}$ mouse and VWM patient brain

We performed polysomal profiling with forebrains of 4-month-old WT and $2b5^{ho}$ mice, shortly before onset of clinical signs in $2b5^{ho}$ mice, when changes in mRNA translation should be detectable, whereas general changes in mRNA translation in response to tissue damage should be minimal.[8] The polysomal profiles from WT and $2b5^{ho}$ samples were similar, showing that bulk mRNA translation was not grossly affected by the mutation (Fig. S1). Microarray analysis revealed differential distribution between the monosome and polysome fractions of WT and $2b5^{ho}$ samples for 33 mRNAs (Data S2), suggesting altered translation rates in $2b5^{ho}$ brain; the majority was shifted toward the polysome fraction in $2b5^{ho}$ brain indicating increased translation efficiencies. Strikingly, 17 of the 33 differentially translated mRNAs are regulated by ATF4 (Fig. 1A),[10] indicating increased ATF4 expression and ATF4-regulated transcription in $2b5^{ho}$ forebrain.

We verified the microarray findings for several candidates with qPCR (Fig. 1B). Most mRNAs with altered translation rates were increased in monosome and polysome fractions from $2b5^{ho}$ mouse brains, indicating that these mRNAs were regulated at transcript level. We focused on differences in mRNA levels within the polysome fractions, without taking into account their distribution between monosome and polysome fractions. We identified 176 mRNAs with altered level of polysome

Figure 1. Polysomal profiling of $2b5^{ho}$ mouse brain identifies ISR deregulation in mouse VWM and human VWM brain. (A) Summary of ISR- and UPR-regulated transcription included to clarify the link between the ATF4, ATF6-c, and XBP1s transcription factors and mRNA targets investigated in this study. (B) ATF4-regulated mRNA levels in gradient fractions from forebrain lysates from 4-month-old WT and $2b5^{ho}$ mice were measured to visualize the mRNA distribution in monosome fraction (A), polysome fractions (B1, less than 5 ribosomes per mRNA; B2, 5 or more ribosomes per mRNA). Graphs show average ± SD, $n = 3$ (*Akt*, qPCR reference). Statistical significance was determined by two-way ANOVA with Sidak's correction; $^{*}P < 0.05$, $^{**}P < 0.01$, $^{****}P < 0.0001$). Raw data for reference mRNAs are shown in Data S7. (C) eIF2α phosphorylation, *Gadd34* and *Crep1* mRNA expression levels were measured in cerebellar tissue from WT and VWM mice, as indicated. Graphs show average ± SD, $n = 3$ for eIF2α phosphorylation and $n = 6$ for mRNA expression (*Gapdh* + *Akt*, qPCR reference). Statistical differences in eIF2α phosphorylation were determined using a one-way ANOVA followed by a Dunnet's correction. Differences between WT and $2b5^{ho}$ qPCR data were assessed with Student's *t*-test, $^{*}P < 0.05$, $^{**}P < 0.01$. (D) *DDIT3*, *TRIB3*, *EIF4EBP1* mRNA levels, eIF2α phosphorylation, *GADD34* and *CREP1* mRNA levels were quantified in postmortem frontal white matter tissue from VWM patients and controls (negative controls without brain pathology, C1, C2, and disease controls CAR and MS; CAR, CARASAL; MS, multiple sclerosis). Expression differences among VWM patients inversely correlate with postmortem delay time (*AKT* + *GAPDH*, qPCR reference, $n = 1$). Details on control and patients' tissue are listed in Data S5. Statistical test outcomes are in Data S6.

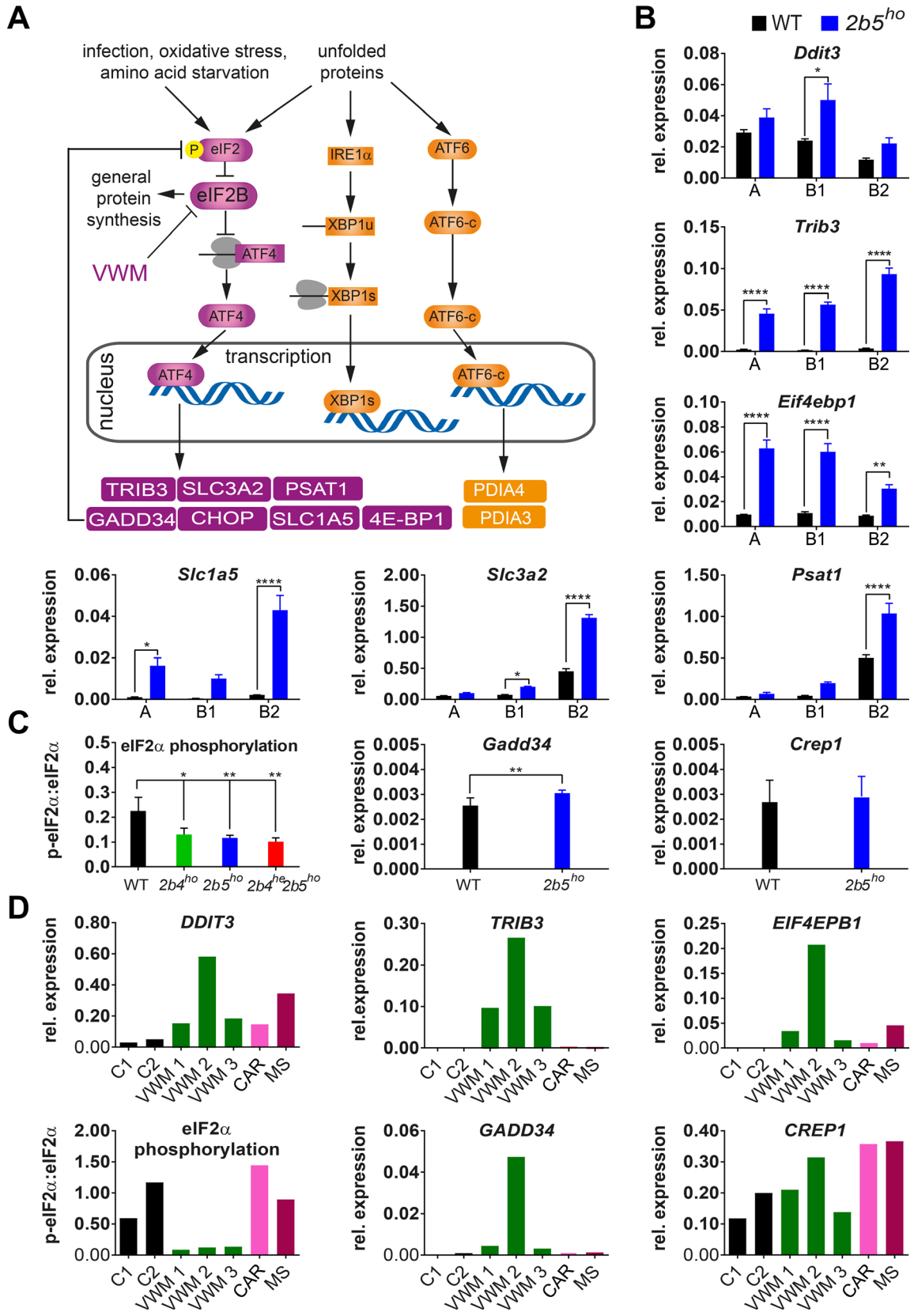

association in *2b5^{ho}* compared to WT forebrain (115 up and 61 down, Data S3), indicating altered synthesis of the encoded proteins. Overrepresentation analysis (Fig. 2A) highlighted changes in amino acid transport, serine biosynthesis and glycine metabolism. Of these 176 mRNAs 52 are regulated by ATF4,[10] including *Ddit3*, which encodes transcription factor CHOP. ATF4-regulated mRNAs were enriched fivefold compared to the mRNAs with similar polysome association in WT and *2b5^{ho}* forebrain ($P < 0.001$; Data S4). We verified findings from mice in humans (Fig. 1D); the expression of ATF4-regulated mRNAs (*DDIT3*, *TRIB3*, and *EIF4EBP1*) was increased in VWM patients' brain. Microarray analyses of total RNA from white matter confirmed a twofold enrichment of ATF4-regulated mRNAs in differentially expressed mRNAs in VWM patients compared to controls ($P < 0.0001$; Data S4).

Expression of the ATF4 transcriptome is accompanied by reduced eIF2α phosphorylation

ATF4 transcriptome expression could be enhanced in VWM brain due to ISR activation via eIF2α phosphorylation. However, we found that eIF2α phosphorylation in brain was significantly reduced in VWM compared to WT mice (Figs. S1C and S2). Dephosphorylation of eIF2α is mediated by protein phosphatase 1, using CREP1 or GADD34 as co-factor.[11] GADD34 is essential for the negative feedback of the ISR (Fig. 1A), whereas CREP1 functions as a cofactor also in unstressed cells.[12] *Gadd34* but not *Crep1* mRNA expression was increased in *2b5^{ho}* brain compared to WT brain (Fig. 1C), in line with its regulation by ATF4 (Fig. 1A).[13] In VWM patients' white matter eIF2α phosphorylation was significantly decreased compared to controls' (Fig. 1D) and *GADD34* but not *CREP1* mRNA levels were increased. The decreased level of eIF2α phosphorylation can be explained by increased expression of GADD34, resulting from increased *Gadd34* mRNA. Western blot analysis for GADD34 protein was unsuccessful.

Activation of all three UPR branches in patients' white matter was previously reported.[14] We investigated activation of the branches regulated by ATF6 or IRE1α in *2b5^{ho}* mouse brain. We measured specific markers for ATF6-driven transcription (*Pdia4* mRNA) and IRE1α activation (*Xbp1* mRNA splicing).[15,16] qPCR analyses did not show increased expression of these markers, arguing against recent or ongoing activation of these UPR branches in *2b5^{ho}* brain (Fig. S3). The previously reported expression of UPR markers in patient brains was determined in end-stage disease.[14] We therefore measured *Pdia4* mRNA expression and *Xbp1* mRNA splicing in *2b5^{ho}* mouse brain at the humane end point, but still did not observe increased expression (Fig. S3). We verified findings in human tissue and found comparable expression of *PDIA3* and *XBP1* splicing in white matter from controls and VWM patients (Fig. S3). Microarray analyses of total RNA from postmortem white matter did not show enrichment of ATF6- and/or IRE1α-regulated mRNAs in differentially expressed mRNAs in VWM patients compared to controls ($P = 0.4507$; Data S4). These findings indicate that eIF2B mutations do not chronically activate ER stress but specifically deregulate ISR homeostasis.

Expression of the ATF4 transcriptome in 2b5^{ho} mouse brain correlates with disease development and severity

We assessed expression levels for several mRNA candidates in mouse brain between postnatal day 0 (P0) and humane end point (Fig. 2B). From P0 to P14 none of the tested candidates differed in the expression between WT and *2b5^{ho}* brain. From P28 onwards the expression of ATF4-regulated mRNAs changed progressively in *2b5^{ho}* but not WT brain ($P < 0.0001$; Fig. 2B). Maximal expression differences were measured at the humane end point.

Figure 2. Follow-up analyses show affected cellular functions and ISR deregulation correlating with disease development. (A) Overrepresentation analysis of regulated polysome-associated mRNAs in *2b5^{ho}* mouse forebrain against the gene ontology (GO) database. # changed, number of mRNAs in GO term differentially associated with *2b5^{ho}* polysomes; # measured, number of mRNAs in GO term detected in WT and *2b5^{ho}* polysomes; # in ontology, total gene number in GO term; results with a *Z* score >2 and FDR of <0.15 were considered significant; fold change, average of differentially expressed genes within the dataset for the particular GO term. (B) Expression of the ATF4-regulated transcriptome in VWM mouse brain correlates positively with disease development. mRNA levels were determined at indicated ages (left hand side) or in indicated genotypes (right hand side). Sagittally sliced brain halves of WT and *2b5^{ho}* mice were analyzed at indicated ages (*Gapdh,* qPCR reference; P, postnatal day; HEP, humane end point, as defined by weight loss of more than 15% of body weight for 2 consecutive days and severe ataxia; 7–8 months of age). Graphs show average ± SD, $n = 2$. Statistical analysis on the differences at groups of different ages was done for each mRNA using a two-way ANOVA (genotype*day interaction all days) followed by 2 two-way ANOVAs for each mRNA (one comparing data of <P21 with ≥P21 and one comparing data of <P28 with ≥P28 for genotype*day interaction) using SPSS. Cerebella of indicated mouse genotypes were analyzed at 4-month-old age (*Gapdh* + *Akt,* qPCR reference). Graphs show average ± SD, $n = 3$ ($n = 4$ for *2b4^{ho}*). Statistical differences were determined using a one-way ANOVA followed by Tukey's correction. $^{**}P < 0.01$, $^{***}P < 0.001$, $^{****}P < 0.0001$ (Data S6).

A

gene ontology name	# changed	# measured	# in GO term	Z score	FDR	fold change
serine family amino acid biosynthetic process	6	8	12	18.64	0.12	3.09
amino acid transmembrane transport	8	33	44	11.81	0.12	3.33
neutral amino acid transport	5	18	23	10.06	0.12	2.64
negative regulation of fatty acid metabolic process	4	13	14	9.51	0.12	2.52
glycine metabolic process	3	10	15	8.12	0.12	2.39
L-amino acid transmembrane transporter activity	5	31	35	7.40	0.12	4.83
vitamin B6 binding	5	41	59	6.26	0.12	1.90
response to organic substance	32	962	1569	5.94	0.12	2.34
positive regulation of cell proliferation	16	380	602	5.21	0.12	1.89

B

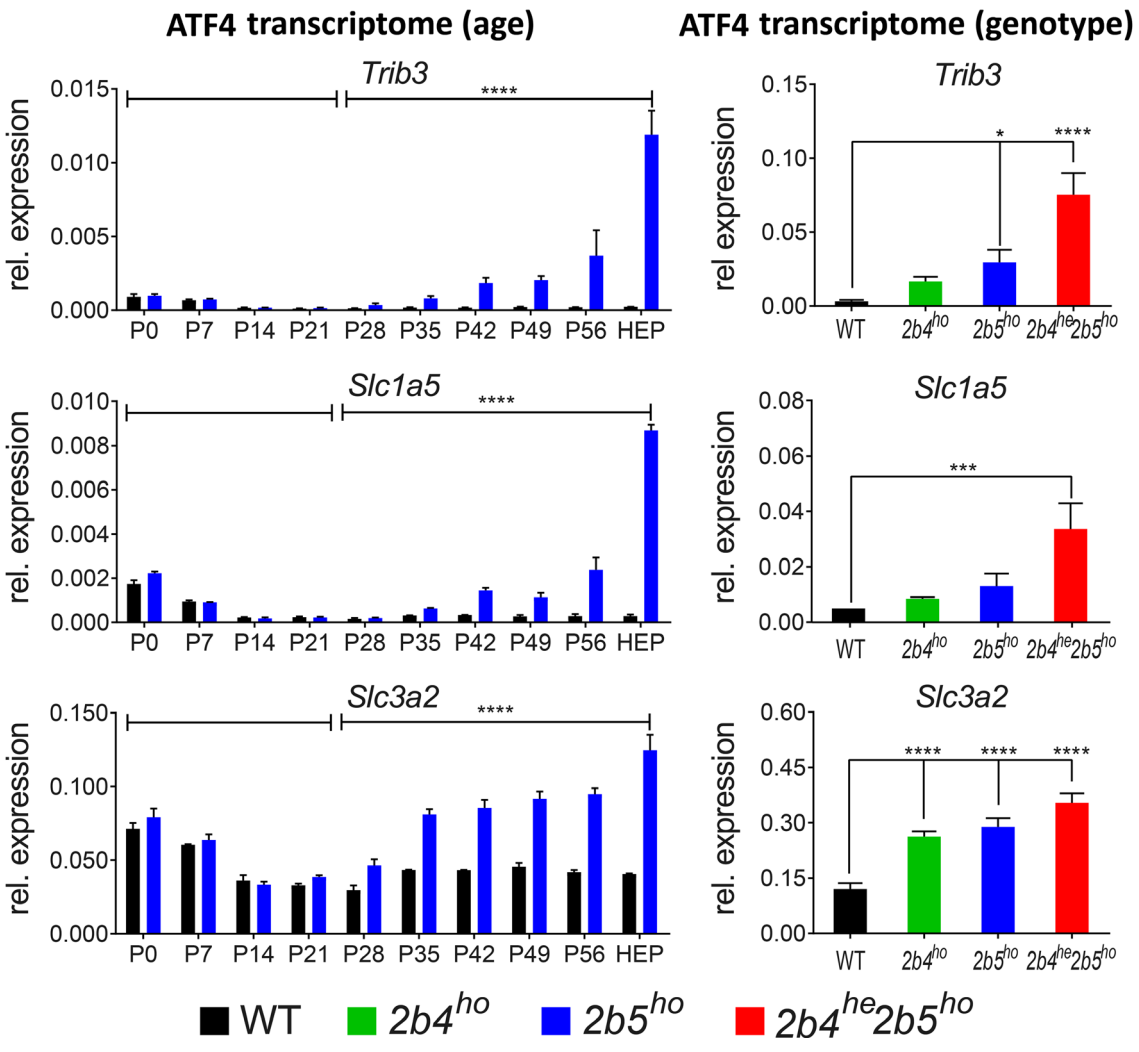

Measuring expression of ATF4-regulated mRNAs in brains of $2b4^{ho}$, $2b5^{ho}$, and $2b4^{he}2b5^{ho}$ mice (Fig. 2B),[8] we found that several correlated positively with disease severity. We did not detect ISR mRNA marker expression in brains of an unrelated neurodegenerative mouse model (Fig. S4).[17] Brain tissue from patients with multiple sclerosis (MS)[18] or cathepsin A-related arteriopathy with strokes and leukoencephalopathy (CARASAL)[19] did not show consistently altered expression of ISR markers (Fig. 1D), indicating that ISR deregulation is not a general event in white matter disease.

ATF4 and 4E-BP1 expression in white and gray matter astrocytes

To identify which specific cells or brain areas display ATF4 transcriptome expression we performed immunohistochemistry for ATF4 and ATF4-regulated 4E-BP1[10,20] on WT and VWM mouse brain (Fig. 3). Antibodies for CHOP, TRIB3, and SLC3A2 did not yield specific signals. Immunohistochemistry for ATF4 showed nuclear ATF4 immunoreactivity in cerebellum, corpus callosum, and cortex in $2b5^{ho}$ but not WT brain (Fig. 3). The morphology of ATF4-positive nuclei, based on size, degree of chromatin compaction, and presence of nucleoli, indicates that the positive cells are macroglia. 4E-BP1 immunoreactivity was observed in white and gray matter cells of cerebellum, corpus callosum, and cortex for $2b4^{ho}$, $2b5^{ho}$, and $2b4^{he}2b5^{ho}$, but not WT mouse brain (Fig. 3). The latter is expected as 4E-BP1 is not expressed in WT brain[21]. Cells were already 4E-BP1-positive in a 1-month-old $2b5^{ho}$ mouse, in line with qPCR findings (Fig. 2B, Fig. S5). The morphology of the 4E-BP1-positive cells corresponded to white and gray matter astrocytes, including Bergmann glia. Double stainings with antibodies against ATF4 or 4E-BP1 and astrocyte marker GFAP revealed ATF4-GFAP and 4E-BP1-GFAP double-positive cells in brain sections of $2b4^{he}2b5^{ho}$ or $2b5^{ho}$ but not WT mice (Fig. 4). All GFAP-positive cells were ATF4-positive in $2b4^{he}2b5^{ho}$ brain sections. No 4E-BP1-positive cells with the morphology of oligodendrocytes were detected in $2b4^{ho}$, $2b5^{ho}$, and $2b4^{he}2b5^{ho}$ brain, even at humane end point (Figs. 3 and 4). Double stainings with antibodies against 4E-BP1 and Olig2, marker for oligodendrocytes[22], did not show any double-positive cells in $2b5^{ho}$ mouse brain (Fig. 4). Double stainings with antibodies against Olig2 and ATF4 to investigate ATF4 expression in oligodendrocytes are infeasible, as the Olig2 signal is much higher than the ATF4 signal and both signals localize in the nuclei. 4E-BP1 signal localizes in the cytoplasm, favoring Olig2-4E-BP1 co-staining.

4E-BP1-positive cells with the morphology of astrocytes were also detected in the frontal white matter, cerebellum, and cortex of brain tissue from VWM patients (Fig. 3); 4E-BP1-positive cells with the morphology of oligodendrocytes or neurons were not observed. 4E-BP1-positive astrocytes, oligodendrocytes or neurons were not observed in brains from one MS and two CARASAL patients (Fig. S6). Staining with ATF4 antibody was unsuccessful in human brain.

ISRIB injections differentially normalize clinical signs of VWM mice

We postulate that the expression of ATF4 transcriptome in astrocytes underlies their dysfunction. To reduce expression of the ATF4 transcriptome we targeted the ISR with ISRIB[9,23–26]. We used $2b5^{ho}$ and $2b4^{ho}2b5^{he}$ genotypes to determine ISRIB's effects on a moderate and severe variant of VWM and on both mutations.

ISRIB increased VWM but not WT mouse body weight compared to placebo-injected controls (Fig. 5A and Fig. S7). Weight gain was fastest and highest in $2b4^{ho}2b5^{he}$ mice. Neurological deterioration as assessed by neuroscores[27] was observed in placebo-treated $2b5^{ho}$ and $2b4^{ho}2b5^{he}$ mice after 18–20 or 11–12 weeks of injections (Fig. 5B). ISRIB-treated $2b5^{ho}$ mice showed signs of mild neurological deterioration toward the end, whereas ISRIB-treated $2b4^{ho}2b5^{he}$ mice did not show neurological signs for the duration of the experiment (Fig. 5B). Motor tests at the end of the experiment revealed that ISRIB improved performance of VWM mice in Balance Beam tests (Fig. 5C). All static and dynamic gait parameters in the catwalk were more affected in placebo-treated $2b4^{ho}2b5^{he}$ mice than placebo-treated $2b5^{ho}$ mice (Fig. 5D, Fig. S8). ISRIB normalized all gait parameters in $2b4^{ho}2b5^{he}$ mice (Fig. 5D; Data S6). ISRIB effects on gait

Figure 3. White and gray matter astrocytes in VWM mice and VWM patients are immunoreactive for ATF4-regulated 4E-BP1. (A) ATF4 immunoreactive nuclei (brown) are detected in white and gray matter macroglia of VWM mice. Two sections from brain tissue from 4-month-old WT and $2b5^{ho}$ mice ($n = 2$) were stained with antibodies against ATF4. Findings in cerebellum, corpus callosum, and cortex are indicated. Staining for ATF4 on human brain sections was not successful. (B) White and gray matter astrocytes in VWM mouse and VWM human brain in show 4E-BP1 immunoreactivity (brown). Two brain sections from 4-month-old mice (WT, $2b5^{ho}$, and $2b4^{he}2b5^{ho}$), human control (C1) or patients (VWM 1 and VWM 2) were stained with antibodies against 4E-BP1. Details on human brain tissue are listed in Data S5. Findings in cerebellum, corpus callosum (mouse) or frontal white matter (WM, human) and cortex are shown. Purple stain indicates nuclei. White bar, 0.05 mm.

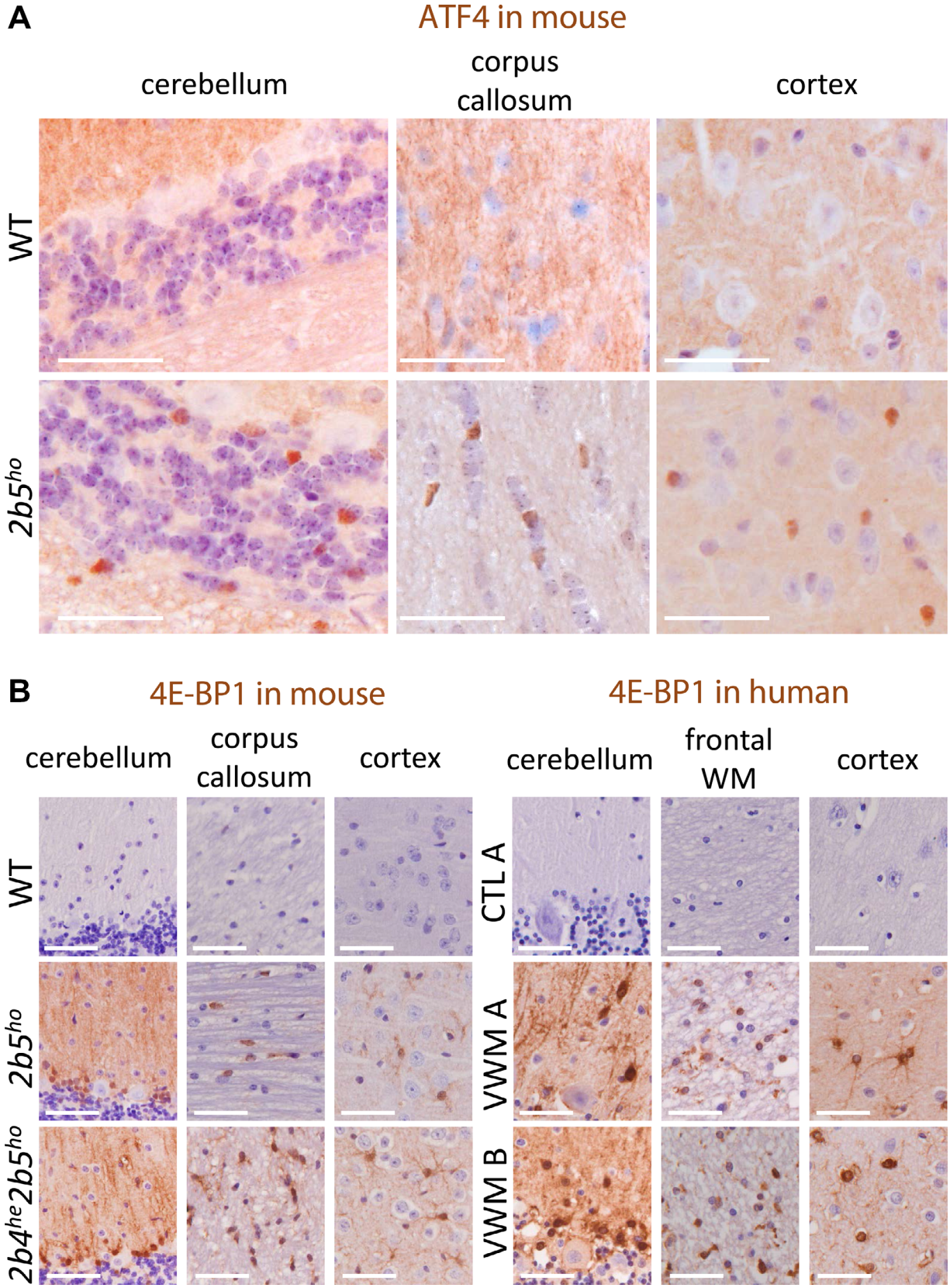

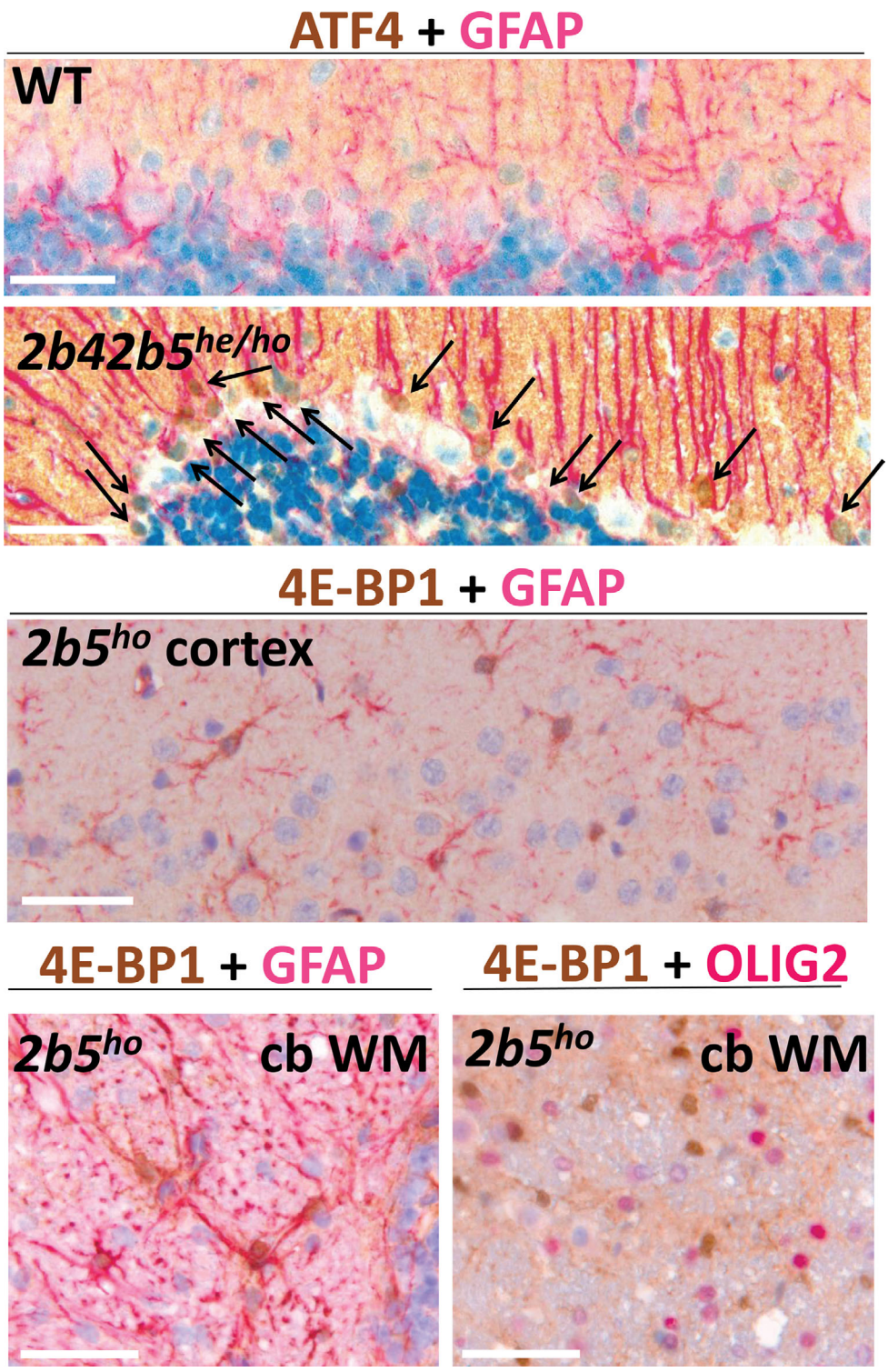

Figure 4. Costaining for ATF4 or 4E-BP1 with GFAP or OLIG2 demonstrate double positive cells of astrocyte but not oligodendrocyte lineage in VWM mice. ATF4-GFAP costaining was only successful on sections from $2b4^{he}2b5^{ho}$ mice (4-month-old). Arrows indicate nuclei of double positive Bergmann glia. Shown are representative sections from a total of four sections (n = 2 animals per group). 4E-BP1 + GFAP staining of astrocytes in cortex is at 2-month-old age. 4E-BP1 + GFAP and 4E-BP1 + OLIG2 double staining of cerebellar white matter (cb WM) is at an age of 12 months (HEP, $2b5^{ho}$). Double positive astrocytes were prominent, whereas oligodendrocytes were not detected, even at HEP. Shown are representative sections from a total of 3–4 sections (n = 2 animals per group).

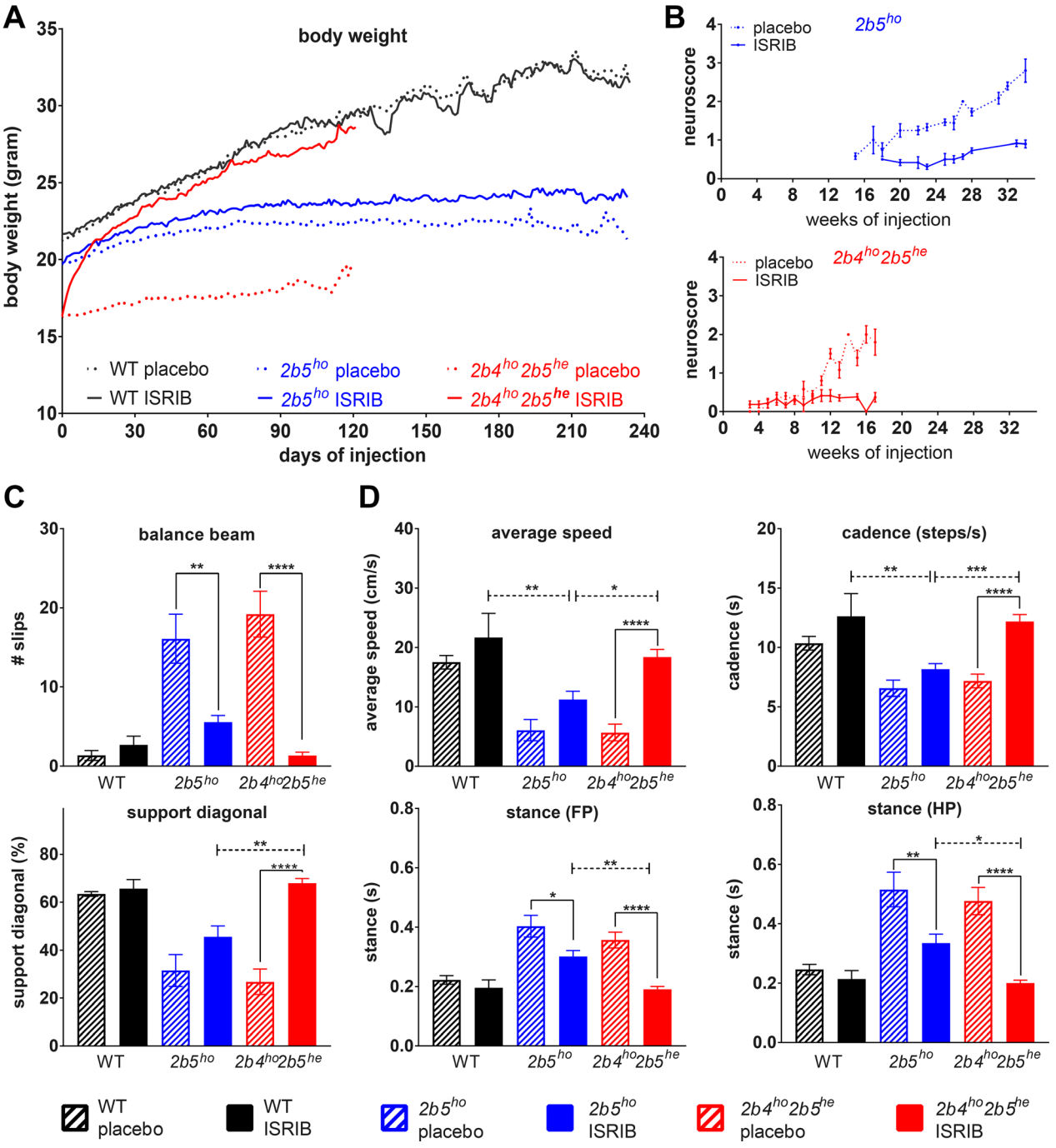

Figure 5. ISRIB ameliorates clinical signs in two VWM mouse models, most effectively in $2b4^{ho}2b5^{he}$ mice. Mice were injected daily with vehicle or 1 mg/kg ISRIB from an age of 6–8 weeks onwards. (A–D) Graphs show phenotypic measures of placebo- and ISRIB-treated WT (n = 6 per condition) and VWM mice ($2b5^{ho}$ and $2b4^{ho}2b5^{he}$ n = 14 per condition or as indicated): average body weight of WT and VWM mice (A), average neuroscore in VWM mice (B), average number of slips on balance beam ($2b5^{ho}$ n = 11 for placebo, n = 13 for ISRIB and $2b4^{ho}2b5^{he}$ n = 10 for placebo and n = 13 for ISRIB, (C), average measures of selected CatWalk parameters ($2b5^{ho}$ n = 9 for placebo, n = 13 for ISRIB and $2b4^{ho}2b5^{he}$ n = 12 for placebo and n = 14 for ISRIB, (D). Error bars indicate SD (graph b), SEM (graphs in c, d), or are left out (graph in a) to allow visualization of the mean values (SEM is shown in Data S6). Raw data of all CatWalk parameters are given in Data S6. Statistical analysis investigating the ISRIB differences in WT, $2b5^{ho}$ and $2b4^{ho}2b5^{he}$ was performed with a two-way ANOVA with Tukey's correction (Data S6). *P < 0.05, **P < 0.01, ***P < 0.001, ****P < 0.0001.

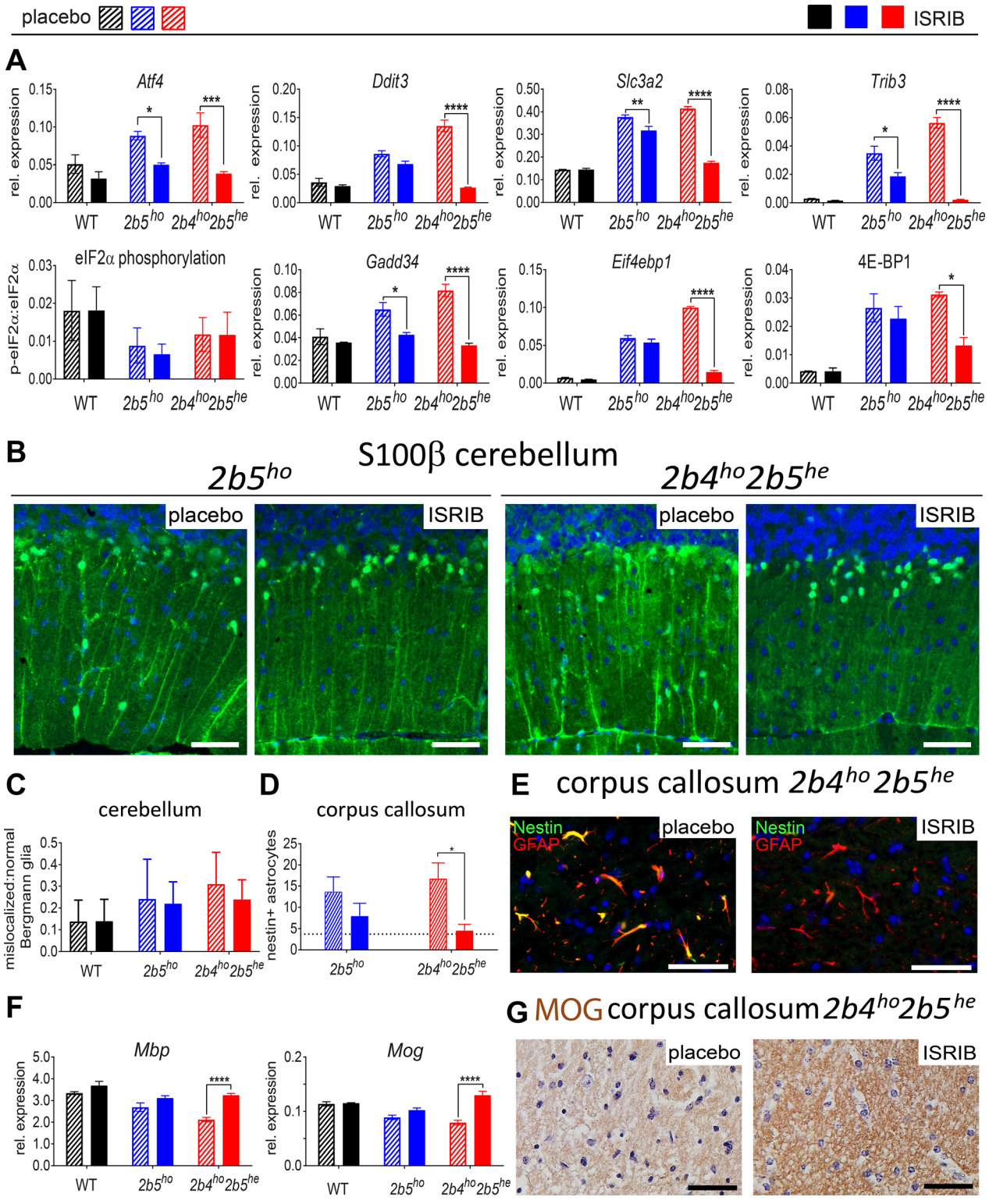

parameters were less consistent and less pronounced in $2b5^{ho}$ than in $2b4^{ho}2b5^{he}$ mice (Fig. 5D, Fig. S8). ISRIB did not affect any parameters in WT mice (Fig. 5D, Fig. S8).

Figure 6. ISRIB modulates aberrant expression of ATF4-regulated mRNAs and ameliorates neuropathological astrocyte markers in VWM mouse cerebellum and corpus callosum. (A) Cerebellar expression of ATF4-regulated mRNAs, eIF2α phosphorylation, and 4E-BP1 protein expression were measured in placebo- and ISRIB-treated WT and VWM mice (n = 6 per group). Graphs show average ± SD. Two-way ANOVA with Tukey's correction was performed for each target. (B) Brain sections from placebo- and ISRIB-treated $2b5^{ho}$ and $2b4^{ho}2b5^{he}$ mice (n = 2 per group, 2 sections per animal) were stained with antibodies against S100β. Thickness of Bergmann glia (BG) processes is reduced by ISRIB in $2b4^{ho}2b5^{he}$ mice; white bar, 0.05 mm. (C) Counts of mislocalized and normally localized S100β-positive Bergmann glia shows that ISRIB does not fully normalize Bergmann glia location in VWM mice. Differences in the ratio of mislocalized:normal localized Bergmann glia were statistically assessed by two-way ANOVA with Tukey's correction. (D and E) ISRIB reduces number of nestin-GFAP double positive astrocytes in $2b4^{ho}2b5^{he}$ mice (2 sections per rostrum and splenium of the corpus callosum for 2 animals per group). The average number of nestin-GFAP double positive astrocytes in four untreated WT animals was included as reference (indicated as dotted line in the graph). Statistical differences were determined with one-way ANOVA using Tukey's correction. White bar in immunofluorescence, 0.05 mm. (F) ISRIB restored levels of mature myelin mRNA markers in $2b4^{ho}2b5^{he}$ mice. Graphs show average ± SD (*Akt* + *Gapdh,* qPCR reference). Two-way ANOVA was performed for each target using Tukey's correction. (G) ISRIB restores immunoreactivity for mature myelin protein MOG in white matter structures in $2b4^{ho}2b5^{he}$ mice. Shown are representative sections from a total of four sections (n = 2 mice per group). Black bar, 0.05 mm. For all graphs, $*P < 0.05$, $**P < 0.01$, $***P < 0.001$, $****P < 0.0001$. Statistical test outcomes are in Data S6.

ISRIB impacts expression of ISR mRNA markers and improves histopathology

ISRIB reduced expression of *Atf4* and ATF4-regulated mRNAs in the brains of VWM mice, most consistently in $2b4^{ho}2b5^{he}$ mice (Fig. 6A). ISRIB did not affect eIF2α phosphorylation levels in $2b5^{ho}$ and $2b4^{ho}2b5^{he}$ mice, despite reduced *Gadd34* mRNA levels (Fig. 6A). ISRIB reduced *Eif4ebp1* mRNA and 4E-BP1 protein expression in ISRIB-injected $2b4^{ho}2b5^{he}$ mice (Fig. 6A), which was not observed in ISRIB-injected WT or $2b5^{ho}$ animals.

Bergmann glia localization in VWM mouse brain was improved by ISRIB more clearly in $2b4^{ho}2b5^{he}$ than in $2b5^{ho}$ mice (Fig. 6B). Bergmann glia were localized closer to the Purkinje cell bodies with ISRIB treatment, but did not reach or maintain their normal position completely (Fig. 6B), causing quantification of the changes in proportion of mislocalized Bergmann glia not reaching significance (Fig. 6C).

The number of nestin and GFAP double-positive immature astrocytes normalized in ISRIB-injected $2b4^{ho}2b5^{he}$ mice and was reduced in $2b5^{ho}$ mice, although statistical significance was not reached for the latter (Fig. 6D and E). ISRIB effects on myelin in VWM mice were evident in mature myelin *Mbp* and *Mog* mRNA levels, MBP protein levels and MOG immunohistochemistry in $2b4^{ho}2b5^{he}$ mice only (Fig. 6F and G, Fig. S9). *Olig2* mRNA levels were similar in all groups (Fig. S9). No ISRIB effects on histology were observed in WT mice (not shown).

ISRIB concentrations in venous blood drawn after 2 weeks of injections were similar in $2b5^{ho}$ and $2b4^{ho}2b5^{he}$ mice albeit lower than in WT mice (Fig. 7A). ISRIB's concentrations in postmortem blood and brain samples were similar in all three genotypes and are well above ISRIB's reported half maximal effective concentration (EC50) of 0.75nM (corresponding to 0.35ng/ml; Fig. 7B)[28], indicating that ISRIB's differential effect on phenotypic measures in $2b5^{ho}$ versus $2b4^{ho}2b5^{he}$ mice cannot be attributed to differences in ISRIB bioavailability in brain. ISRIB's therapeutic effect may be influenced by the specific mutation. A recent study shows that ISRIB's EC50 is decreased by the Arg483Trp mutation in human eIF2Bδ.[28] We measured ISRIB's effect on protein synthesis rates in cultured astrocytes from WT, $2b5^{ho}$ and $2b4^{ho}2b5^{he}$ mice undergoing a UPR (Fig. 7C). ISRIB appeared more effective in $2b4^{ho}2b5^{he}$ than in WT and $2b5^{ho}$ astrocytes (Fig. 7C), although the number of measurements is limited.[29] We also found that protein synthesis in transfected $2b4^{ho}2b5^{he}$ astrocytes was more sensitive to low concentrations of ISRIB than transfected WT astrocytes (Fig. 7D; 4–6 measurements). Increased ISRIB sensitivity was not observed in $2b5^{ho}$ astrocytes (Fig. 7D).

Discussion

One study objective was to contribute to unraveling VWM pathophysiology, a leukodystrophy characterized by primary astrocyte pathology.[8] With VWM mice we study the chronic disease; acute deteriorations have not been modeled yet.[29] We demonstrate increased expression of ATF4-regulated transcriptome in $2b5^{ho}$ brain from before disease onset. Its expression level correlates with disease development and severity. Strikingly, this ATF4-regulated transcriptome is expressed selectively in astrocytes and not in other cell types in VWM mouse and patient brain; it is specific for VWM and not a general response to white matter disease.

Our study disproves the concept that the UPR is activated in VWM[30]. Reduced phosphorylated eIF2α in $2b5^{ho}$ mouse and VWM patient brains argues against cell stress as initiating event; reduced activity of mutant eIF2B by itself can explain the increased expression of ATF4 and its transcriptome, including *Gadd34*.[3] Increased GADD34 can explain the decrease in phosphorylated eIF2α. That

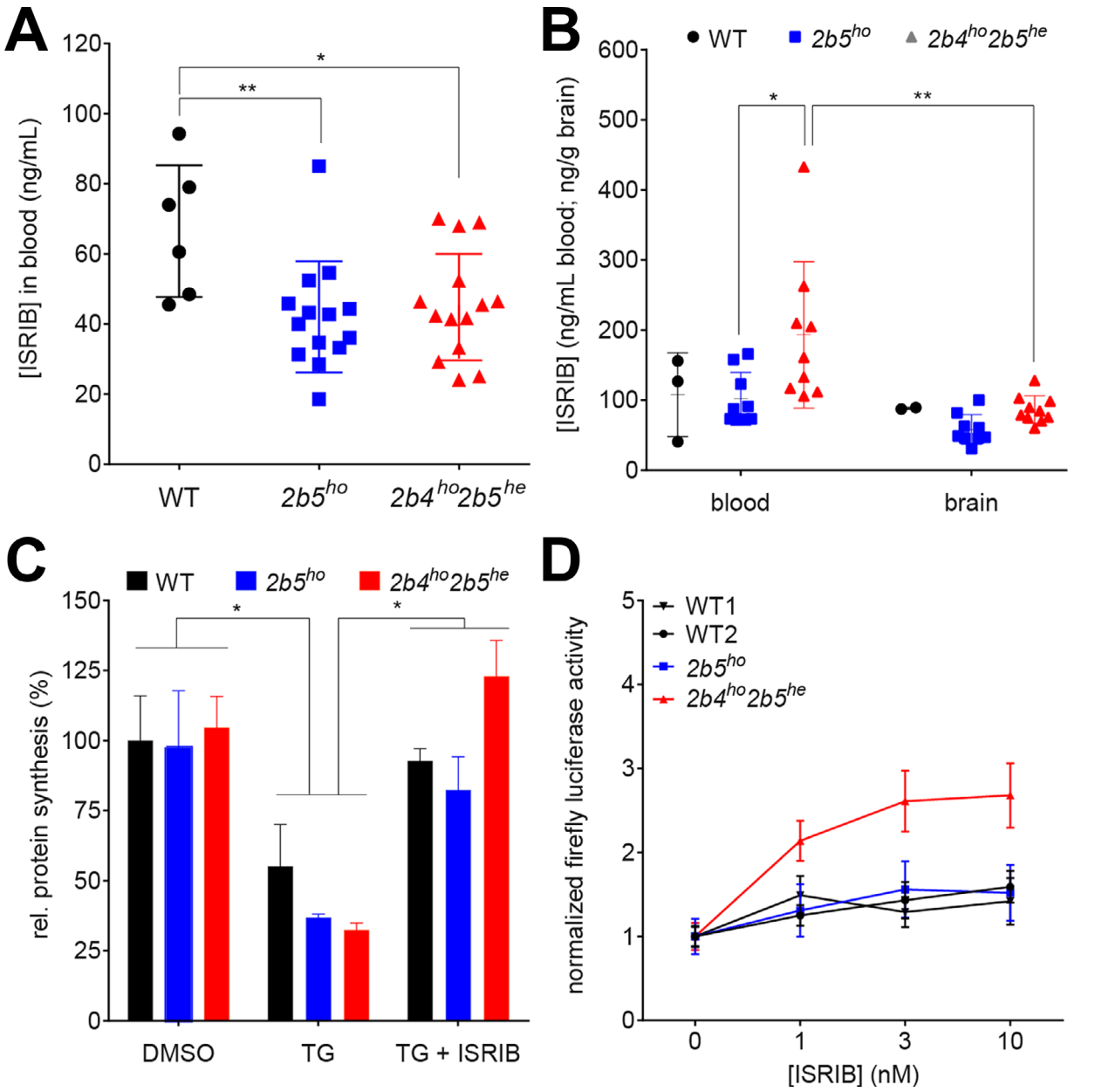

Figure 7. ISRIB's efficacy in VWM is influenced by the identity of eIF2B mutation. (A) ISRIB concentrations were determined in venous blood samples obtained from WT (n = 6 per group) and VWM mice ($2b5^{ho}$ and $2b4^{ho}2b5^{he}$ n = 14 per group) after 14 days of daily ISRIB injections (24 h after the latest injection); data obtained from placebo-treated animals were below detection and were omitted from the graph. Statistical differences among genotypes were determined with one-way ANOVA followed by Tukey's correction. (B) ISRIB concentrations were determined in postmortem blood and olfactory bulb tissue from WT (n = 2 per group) and VWM mice ($2b5^{ho}$ and $2b4^{ho}2b5^{he}$ n = 9 and n = 8 per group). Statistical differences were determined with Two-way ANOVA (tissue and genotype as factors) with Tukey's correction. (C) ISRIB restored protein synthesis rates in primary cultures of adult mouse astrocytes undergoing UPR, most effectively in cells from $2b4^{ho}2b5^{he}$ mice. TG effects were not statistically significant as before[29]. Statistical differences in test conditions (DMSO vs. TG vs. TG + ISRIB within WT, $2b5^{ho}$, and $2b4^{ho}2b5^{he}$ adult mouse astrocytes were determined with two-way ANOVA with Tukey's correction (n = 2). (D) ISRIB enhanced expression of *Gapdh*-driven firefly luciferase reporter in $2b4^{ho}2b5^{he}$ astrocytes at lower concentrations than in WT or $2b5^{ho}$ astrocytes (P = 0.0026). WT1 and WT2 indicate different isolation dates. Cells were exposed to 300 nmol/L thapsigargin for 16 h with increasing concentrations of ISRIB. Areas under curve (AUC) were calculated for each cell isolate per transfection experiment after correcting for differences between experiments but not between test conditions within experiments (genotype, treatments). Statistical differences between ISRIB sensitivity in WT1, WT2, $2b5^{ho}$, and $2b4^{ho}2b5^{he}$ adult mouse astrocytes were determined with one-way ANOVA with Sidak's correction using AUC values. For all panels, $*P < 0.05$, $**P < 0.01$. Statistical test outcomes are in Data S6. Graphs show mean ± SD (A–C) or mean ± SEM (D).

eIF2α phosphorylation is reduced below baseline indicates a constitutively activated feedback mechanism. Considering that ATF4 is still expressed, reduced eIF2α phosphorylation is apparently unable to fully compensate reduced eIF2B activity. With complete compensation, ATF4 levels would have been similar in WT and VWM brain. Together our findings reveal a constitutively and increasingly deregulated ISR homeostasis in VWM. Recently, others have reported normal eIF2α phosphorylation in *2b5^{ho}* mice[31], which may be ascribed to technical variation, as the phosphorylated eIF2α signal is fairly low.[31]

We previously demonstrated that guanabenz improves white matter and astrocyte pathology in *2b5^{ho}* mice.[32] Guanabenz is an α2-adrenergic receptor agonist that also targets the ISR and reduces expression of ATF4-regulated transcriptome[27]. We now demonstrate that ISRIB, which activates eIF2B and thereby reduces expression of the ATF4-regulated transcriptome, improves white matter and astrocyte pathology and ameliorates the clinical disease in VWM mice, arguing against the α2-adrenergic receptor as mechanism through which guanabenz had its impact on VWM.

We conclude that reduced activity of mutant eIF2B initiates the disease in VWM. It increases expression of ATF4 and ATF4-regulated transcriptome, which is moderated through the GADD34 feedback loop, decreasing eIF2α phosphorylation to even below control level. The latter is insufficient to normalize eIF2B activity, resulting in constitutive and increasing activation of the ATF4 transcriptome, causing disease.

In line with a previous study[23], ISRIB did not affect eIF2α phosphorylation in VWM mice. A rise in eIF2 phosphorylation would have been expected, as ISRIB reduced *Gadd34* mRNA levels. Possibly, the ISRIB-induced reduction in GADD34 protein level was not sufficient to achieve this. The ATF4 expression was not completely normalized either by ISRIB, as exemplified by 4E-BP1 protein expression still being detected in brain tissue of ISRIB-treated VWM mice (Fig. 6). Both findings suggest that ISRIB treatment does not fully normalize eIF2B activity, but leads to a better compensated system that still in part depends on reduced eIF2α phosphorylation.

ISRIB stabilizes the eIF2B complex formation through interaction with the eIF2Bδ:eIF2Bβ interface[33,34]. Its effect may be influenced by the specific VWM mutation. The eIF2Bδ Arg483Trp mutation is close to the ISRIB-binding site[33] and may enhance ISRIB binding. The eIF2Bδ Arg483Trp mutation also interferes with eIF2B complex stability[3], whereas the eIF2Bε Arg195His mutation does not and possibly reduces eIF2B activity through another mechanism.[35] ISRIB may preferentially impact eIF2B with complex-destabilizing mutations.

The question how ISR deregulation causes pathology remains difficult to answer. Our overrepresentation analyses on regulated mRNAs in *2b5^{ho}* mouse brain highlight increased functions of amino acid transport and biosynthesis of serine, glycine and cysteine. Several related genes are regulated by ATF4.[10] Increased serine and glycine levels have been reported in cerebrospinal fluid of VWM patients[36], indicating that the identified functions are indeed likely deregulated. Interestingly, serine, glycine, and cysteine are used with glutamate for synthesis of the antioxidant glutathione (GSH).[37] The ATF4-regulated transcription is known to aid in counteracting reactive oxygen species (ROS).[38] ROS typically induce eIF2α phosphorylation.[39] In brains of VWM mice and VWM patients, eIF2α phosphorylation is low, suggesting that ROS levels are not enhanced. The ATF4-induced increased synthesis and secretion of GSH by astrocytes may thus induce reductive shifts in the steady-state redox potential[40], which may inhibit maturation of oligodendrocyte precursor cells.[41] Strikingly, an astrocyte-dependent impairment of oligodendrocyte maturation is a central feature of VWM.[2,8] All data combined suggest that the defect in oligodendrocyte maturation may be due to a reductive shift in redox potential in mutant astrocytes induced by ISR-deregulation (Fig. S10).

We achieved our second objective by confirming that ISR modulation can improve VWM. ISRIB targets eIF2B from various species, ranging from mice to humans[9,25,33], indicating that ISRIB is probably also efficacious in VWM patients. ISRIB's effect may be influenced by the specific eIF2B mutations and it may not be equally effective in all patients. Testing ISRIB on patient cells before prescription may be required. Additionally, ISRIB has low solubility and its bioavailability in humans needs optimization. Recently, a soluble ISRIB derivative (2BAct) was successful in preventing VWM clinical signs and neuropathology in a *2b5^{ho}* mouse model.[31]

We have demonstrated that ISR derangement is central in VWM pathogenesis and that the ISR is a viable drug target for VWM. The role of ISR regulation in health and disease is currently at the center of attention in aging and various neurodegenerative diseases, including Alzheimer disease, Parkinson disease and ALS.[42,43] This study reveals that modulation of ISR deregulation ameliorates neurological dysfunction in VWM mice without affecting general health, indicating the potential of ISRIB for patients with VWM and other conditions characterized by abnormal ISR activation.

Acknowledgments

Financial support for the study was provided by ZonMw (TOP grants 40-00812-98-11005 and 91217006), NWO (Spinoza award 2008), Fonds NutsOHRA (1204-032),

Hersenstichting (BGWS2014(1)-04), and the European Leukodystrophy Association (grant ELA 2017-02712).

We thank Gerbren Jacobs for mouse genotyping. We thank Dave Speijer for fruitful discussions and critically reading the manuscript. We thank Nienke Wevers, Carola G. M. van Berkel, Gino Hu-A-Ng, Erwin E. W. Janssen, Herman ten Brink, Ilja Boor and Bastijn Koopmans for technical assistance. We thank Pim van Nierop for advice on overrepresentation analyses. We thank the staff of the VU mouse housing facility for mouse breeding and injections. We thank Maarten Loos for providing access to the CatWalk software. We thank Rogier Min for fruitful discussions during the preparation of the manuscript.

Authors Contribution

MSvdK and TEMA conceptualized the project. AAMT and TEMA developed the protocol for sample and polysome preparation. TEMA and EP performed the polysomal profiling experiments. MB designed the microarray on human brain RNA. MJT and DM performed data analyses and variance analyses of microarray data of mouse brain and human brain. HF and LW performed overrepresentation analyses. LW, EP, NLP, and TJtB performed the qPCR and Western blot experiments. LW and EJ performed the statistical analyses of data acquired with qPCR, Western blot. SvdS designed and advised on statistical methods. NLP performed Immunohistochemistry and immunofluorescence experiments under supervision of MB. MSvdK supervised the use of human and mouse tissue. MV provided the *Gfap-Sca*$^{-/-}$ mice and advised on the experiment design. TEMA designed the ISRIB trial. TJtB, SB, NS, EJ, and TEMA acquired and analyzed data during ISRIB trial, including body weight, neuroscores, balance beam. NS performed CatWalk experiments and analyzed the data. EAS designed and supervised the ISRIB measurements in blood and brain. LW and DVG performed the protein synthesis measurements and the statistical analyses of the acquired data. TEMA and MSvdK wrote the manuscript. TEMA and EJ made the figures.

Conflict of Interest

MSvdK and TEMA have a patent PCT/NL2018/050293 on Guanabenz in VWM pending. Otherwise, the authors have declared that no competing interest exists.

References

1. Hamilton E, van der Lei H, Vermeulen G, et al. The natural history of Vanishing White Matter. Ann Neurol 2018;84:274–288.
2. Bugiani M, Boor I, van Kollenburg B, et al. Defective glial maturation in vanishing white matter disease. J Neuropathol Exp Neurol 2011;70:69–82.
3. Li W, Wang X, Van Der Knaap MS, Proud CG. Mutations linked to leukoencephalopathy with vanishing white matter impair the function of the eukaryotic initiation factor 2B complex in diverse ways. Mol Cell Biol 2004;24:3295–3306.
4. Liu R, van der Lei HD, Wang X, et al. Severity of vanishing white matter disease does not correlate with deficits in eIF2B activity or the integrity of eIF2B complexes. Hum Mutat 2011;32:1036–1045.
5. Leegwater PA, Vermeulen G, Konst AA, et al. Subunits of the translation initiation factor eIF2B are mutant in leukoencephalopathy with vanishing white matter. Nat Genet 2001;29:383–388.
6. van der Knaap MS, Leegwater PA, Konst AA, et al. Mutations in each of the five subunits of translation initiation factor eIF2B can cause leukoencephalopathy with vanishing white matter. Ann Neurol 2002;51:264–270.
7. Pakos-Zebrucka K, Koryga I, Mnich K, et al. The integrated stress response. EMBO Rep 2016;17:1374–1395.
8. Dooves S, Bugiani M, Postma NL, et al. Astrocytes are central in the pathomechanisms of vanishing white matter. J Clin Invest 2016;126:1512–1524.
9. Sidrauski C, Tsai JC, Kampmann M, et al. Pharmacological dimerization and activation of the exchange factor eIF2B antagonizes the integrated stress response. Elife 2015;4:e07314.
10. Han J, Back SH, Hur J, et al. ER-stress-induced transcriptional regulation increases protein synthesis leading to cell death. Nat Cell Biol 2013;15:481–490.
11. Jousse C, Oyadomari S, Novoa I, et al. Inhibition of a constitutive translation initiation factor 2alpha phosphatase, CReP, promotes survival of stressed cells. J Cell Biol 2003;163:767–775.
12. Marciniak SJ, Yun CY, Oyadomari S, et al. CHOP induces death by promoting protein synthesis and oxidation in the stressed endoplasmic reticulum. Genes Dev 2004;18:3066–3077.
13. Novoa I, Zeng H, Harding HP, Ron D. Feedback inhibition of the unfolded protein response by GADD34-mediated dephosphorylation of eIF2alpha. J Cell Biol 2001;153:1011–1022.
14. van Kollenburg B, van Dijk J, Garbern J, et al. Glia-specific activation of all pathways of the unfolded protein response in vanishing white matter disease. J Neuropathol Exp Neurol 2006;65:707–715.
15. Wu J, Rutkowski DT, Dubois M, et al. ATF6alpha optimizes long-term endoplasmic reticulum function to protect cells from chronic stress. Dev Cell 2007;13:351–364.
16. Lee AH, Iwakoshi NN, Glimcher LH. XBP-1 regulates a subset of endoplasmic reticulum resident chaperone genes

in the unfolded protein response. Mol Cell Biol 2003;23:7448–7459.
17. Camargo N, Goudriaan A, van Deijk AF, et al. Oligodendroglial myelination requires astrocyte-derived lipids. PLoS Biol 2017;15:e1002605.
18. Ransohoff RM, Hafler DA, Lucchinetti CF. Multiple sclerosis-a quiet revolution. Nat Rev Neurol 2015;11:134–142.
19. Bugiani M, Kevelam SH, Bakels HS, et al. Cathepsin A-related arteriopathy with strokes and leukoencephalopathy (CARASAL). Neurology 2016;87:1777–1786.
20. Yamaguchi S, Ishihara H, Yamada T, et al. ATF4-mediated induction of 4E-BP1 contributes to pancreatic beta cell survival under endoplasmic reticulum stress. Cell Metab 2008;7:269–276.
21. Bidinosti M, Ran I, Sanchez-Carbente MR, et al. Postnatal deamidation of 4E-BP2 in brain enhances its association with raptor and alters kinetics of excitatory synaptic transmission. Mol Cell 2010;37:797–808.
22. Silbereis JC, Huang EJ, Back SA, Rowitch DH. Towards improved animal models of neonatal white matter injury associated with cerebral palsy. Dis Model Mech 2010;3:678–688.
23. Halliday M, Radford H, Sekine Y, et al. Partial restoration of protein synthesis rates by the small molecule ISRIB prevents neurodegeneration without pancreatic toxicity. Cell Death Dis 2015;6:e1672.
24. Hearn BR, Jaishankar P, Sidrauski C, et al. Structure-activity studies of Bis-O-Arylglycolamides: inhibitors of the integrated stress response. ChemMedChem 2016;11:870–880.
25. Sekine Y, Zyryanova A, Crespillo-Casado A, et al. Stress responses. Mutations in a translation initiation factor identify the target of a memory-enhancing compound. Science 2015;348:1027–1030.
26. Sidrauski C, Acosta-Alvear D, Khoutorsky A, et al. Pharmacological brake-release of mRNA translation enhances cognitive memory. Elife 2013;2:e00498.
27. Dickhout JG, Carlisle RE, Jerome DE, et al. Integrated stress response modulates cellular redox state via induction of cystathionine gamma-lyase: cross-talk between integrated stress response and thiol metabolism. J Biol Chem 2012;287:7603–7614.
28. Wong YL, LeBon L, Edalji R, et al. The small molecule ISRIB rescues the stability and activity of Vanishing White Matter Disease eIF2B mutant complexes. Elife 2018;7:e32733.
29. Wisse LE, Ter Braak TJ, van de Beek MC, et al. Adult mouse eIF2Bepsilon Arg191His astrocytes display a normal integrated stress response in vitro. Sci Rep 2018;8:3773.
30. van der Voorn JP, van Kollenburg B, Bertrand G, et al. The unfolded protein response in vanishing white matter disease. J Neuropathol Exp Neurol 2005;64:770–775.
31. Wong YL, LeBon L, Basso AM, et al. eIF2B activator prevents neurological defects caused by a chronic integrated stress response. Elife 2019;8.
32. Dooves S, Bugiani M, Wisse LE, et al. Bergmann glia translocation: a new disease marker for vanishing white matter identifies therapeutic effects of Guanabenz treatment. Neuropathol Appl Neurobiol 2018;44:391–403.
33. Tsai JC, Miller-Vedam LE, Anand AA, et al. Structure of the nucleotide exchange factor eIF2B reveals mechanism of memory-enhancing molecule. Science 2018;359:eaaq0939.
34. Zyryanova AF, Weis F, Faille A, et al. Binding of ISRIB reveals a regulatory site in the nucleotide exchange factor eIF2B. Science 2018;359:1533–1536.
35. Wang X, Wortham NC, Liu R, Proud CG. Identification of residues that underpin interactions within the eukaryotic initiation factor (eIF2) 2B complex. J Biol Chem 2012;287:8263–8274.
36. van der Knaap MS, Wevers RA, Kure S, et al. Increased cerebrospinal fluid glycine: a biochemical marker for a leukoencephalopathy with vanishing white matter. J Child Neurol 1999;14:728–731.
37. Banerjee R. Redox outside the box: linking extracellular redox remodeling with intracellular redox metabolism. J Biol Chem 2012;287:4397–4402.
38. Harding HP, Zhang Y, Zeng H, et al. An integrated stress response regulates amino acid metabolism and resistance to oxidative stress. Mol Cell 2003;11:619–633.
39. Liu L, Wise DR, Diehl JA, Simon MC. Hypoxic reactive oxygen species regulate the integrated stress response and cell survival. J Biol Chem 2008;283:31153–31162.
40. McBean GJ. Cysteine, glutathione, and thiol redox balance in astrocytes. Antioxidants (Basel) 2017;6:62.
41. Smith J, Ladi E, Mayer-Proschel M, Noble M. Redox state is a central modulator of the balance between self-renewal and differentiation in a dividing glial precursor cell. Proc Natl Acad Sci USA 2000;97:10032–10037.
42. Hughes D, Mallucci GR. The unfolded protein response in neurodegenerative disorders - therapeutic modulation of the PERK pathway. FEBS J 2018;e14422.
43. Scheper W, Hoozemans JJ. The unfolded protein response in neurodegenerative diseases: a neuropathological perspective. Acta Neuropathol 2015;130:315–331.

Supporting Information

Additional supporting information may be found online in the Supporting Information section at the end of the article.

Figure S1. Polysome profiles of wild type and *2b5ho*mouse brain are similar.
Figure S2. Raw data for quantifying eIF2α phosphorylation using Western blot.

Figure S3. The ATF4-transcriptome is expressed in VWM mouse and VWM patients' brain without markers indicating cellular stress.
Figure S4. Absence of enhanced expression of ATF4-regulated mRNAs in brain tissue from *Gfap-Scap*$^{-/-}$ mice.
Figure S5. White and grey matter astrocytes in VWM mice are immunoreactive for ATF4-regulated 4E-BP1 before clinical signs.
Figure S6. Absence of 4E-BP1 immunoreactive astrocytes, oligodendrocytes or neurons in brain sections from MS and CARASAL patients.
Figure S7. ISRIB ameliorates reduced body weight in two VWM mouse models, most effectively in *2b4ho2b5he* mice.
Figure S8. ISRIB ameliorates gait abnormalities in two VWM mouse models, most effectively in *2b4ho2b5he* mice; additional data of WT and VWM mice treated with placebo or ISRIB.
Figure S9. Additional quantification of myelin markers by qPCR and Western blot.
Figure S10. Molecular model for failing oligodendrocyte maturation in VWM and molecular effects of ISRIB.
Data S1. qPCR primers and antibodies.
Data S2. eIF2Bε^{Arg191His}–regulated shifts in mouse forebrain polysome association.
Data S3. Polysome association in *2b5*^{ho} mouse brain differs for 176 mRNAs.
Data S4. Enrichment of ER stress pathway – Results fishers exact test Mouse and Human.
Data S5. Patient information.
Data S6. Results statistical analyses.
Data S7. Raw qPCR data for reference mRNAs polysomal profiling.

